# The Mechanical Behavior of Metal-Halide Perovskites: Elasticity, Plasticity, Fracture, and Creep

Zhenghong Dai [1], Meaghan C. Doyle [1], Xing Liu [1], Mingyu Hu [1], Qizhong Wang [1], Christos E. Athanasiou [1], Yucheng Liu [2], Brian W. Sheldon [1], Huajian Gao [1,3,4], Shengzhong (Frank) Liu [2], Nitin P. Padture [1,*]

[1] School of Engineering, Brown University, Providence, RI 02912, USA
[2] School of Materials Science and Engineering, Shaanxi Normal University, Xi'an 710119, China
[3] School of Mechanical and Aerospace Engineering, College of Engineering, Nanyang Technological University, Singapore 639798, Singapore
[4] Institute of High Performance Computing, A*STAR, Singapore 138632, Singapore

[*] Email: nitin_padture@brown.edu

For: *Scripta Materialia* (Manuscript # SMM-22-1455)

**Abstract**

Wide ranging mechanical properties — elasticity, plasticity, fracture, and creep — most relevant to the mechanical reliability of perovskite solar cells (PSCs) are systematically investigated. High quality bulk single-crystals of the commonly studied metal halide perovskites (MHPs) relevant to PSCs are fabricated and studied: $CH_3NH_3PbBr_3$ ($MAPbBr_3$) and $CH_3NH_3PbI_3$ ($MAPbI_3$). The first direct measurement of MHP Young's modulus ($E$) using uniaxial compression reveals $E_{<100>}$ of 13.1±1.3 and 10.6±1.0 GPa for $MAPbBr_3$ and $MAPbI_3$, respectively. The Vickers micro-hardness $H_{(100)}$ of $MAPbBr_3$ and $MAPbI_3$ is 0.54±0.02 GPa and 0.76±0.05 GPa, respectively. The Vickers micro-indentation fracture toughness $K_{IC}$ of $MAPbBr_3$ and $MAPbI_3$ is estimated at 0.20±0.03 MPa·m$^{0.5}$ and 0.18±0.03 MPa·m$^{0.5}$, respectively. The stress-exponent, $n$, extracted from nanoindentation creep data is ~8 and ~10 for $MAPbBr_3$ and $MAPbI_3$, respectively. The trends in these properties are discussed. These properties are best estimates and are recommended for use in future mechanical behavior and reliability analyses of MHPs and PSCs.

**Graphical Abstract**

| Essential Mechanical Properties of Metal Halide Perovskites (MHPs) | 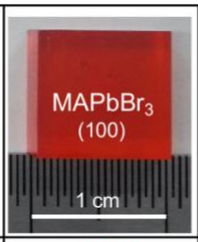  | 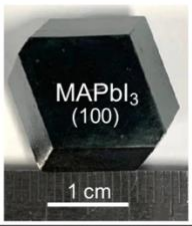  |
|---|---|---|
| $E_{<100>}$ (GPa): | 13.1 | 10.6 |
| $H_{(100)}$ (GPa): | 0.54 | 0.76 |
| $K_{IC}$ (MPa·m$^{0.5}$): | 0.20 | 0.18 |
| $n$ (Creep Exp.): | ~8 | ~10 |

The promise of low cost and high power-conversion efficiency (PCE) has been driving the worldwide effort in the new perovskite solar cells (PSCs) incorporating metal halide perovskite (MHP) light-absorbers.[1, 2] Also, tandem photovoltaics (PVs) incorporating PSCs with even higher efficiencies hold great promise.[3, 4] Thus, PSCs research has focused not only on increasing PCE and upscaling,[5] but also improving stability.[6-8] However, PSCs will also need to be mechanically reliable if they are to operate efficiently for decades,[7, 9-15] but there is a dearth of research in this area. In this context, historically, most commercial devices, including PVs, have gone through a typical research/development trajectory — increasing performance, upscaling, improving stability, and enhancing reliability — before making it to the marketplace successfully; PSCs are likely to be no exception.[16]. In fact, enhancing the mechanical reliability of PSCs is particularly important and challenging because the low formation energies of MHPs render them inherently poor in mechanical properties, relative to their inorganic counterparts such as Si and CdTe, in commercial PVs.[11, 15] Furthermore, PSCs are expected to experience significant mechanical stresses that drive damage accumulation and failure over their lifetime.[11, 15, 17, 18]

In this context, we have investigated here some basic mechanical properties of MHPs most relevant to mechanical reliability: (i) elastic modulus (resistance to elastic deformation), (ii) hardness (resistance to local plastic deformation), (iii) fracture toughness (resistance to crack propagation), and (iv) creep (time-dependent permanent deformation). High quality bulk single-crystals of the commonly studied MHPs relevant to PSCs are fabricated and studied:

methylammonium lead tribromide ($CH_3NH_3PbBr_3$ or $MAPbBr_3$) and methylammonium lead triiodide ($CH_3NH_3PbI_3$ or $MAPbI_3$).

*Elasticity.* Quasi-static Young's modulus ($E$) is perhaps the most basic of the mechanical properties needed for analyzing the mechanical reliability of PSCs, and, therefore, it is critically important to measure it accurately. For example, it is needed to estimate the damage-/failure-driving residual stresses and applied stresses (such as in bending) in the MHP thin film within PSCs, but this property has not been measured directly in MHPs. All the reported experimental $E$ values for MHP bulk single-crystals have been measured using model-dependent indirect methods, with the most popular method being nanoindentation. Table 1 lists single-crystal Young's modulus ($E$) values for $MAPbBr_3$ and $MAPbI_3$ (100) surfaces. These values are in the ranges 17.7-30.2 GPa for $MAPbBr_3$ and 10.4-23.92 GPa for $MAPbI_3$. These wide variations in the $E$ values using the nanoindentation method are attributed to its sensitivity to the following: synthesis method, quality, and orientation of the single-crystals; preparation of the indentation surfaces; geometry and quality of the indenter tip; instrumental effects; indentation parameters used; models and methodologies, used to extract the $E$ values, *etc*. Also, although nanoindentation is performed on (100) surfaces of bulk single-crystals, that does not imply that the measured $E$ is in <100> direction due to the complex three-dimensional (3D) geometry of the elastic recovery process in this method. Note that the $E_{<100>}$ values calculated using density functional theory (DFT) are in the range 20.3-29.1 GPa and 17.2-22.8 GPa for $MAPbBr_3$ and $MAPbI_3$, respectively.[19, 20] The reasons for the overestimation of the $E_{<100>}$ values in Table 1 using high-frequency methods, and also DFT, are not clear. To circumvent all these issues, here we have directly measured the $E_{<100>}$ of $MAPbBr_3$ and $MAPbI_3$ bulk single-crystals using uniaxial compression. High quality cm-sized bulk single-crystals of $MAPbBr_3$ [21] and $MAPbI_3$ [22] were grown using processes described in the Supplementary Material (SM); photographs of examples are shown in Figs. 1a and 1b (insets). They were cut to size and polished, and then tested in uniaxial compression (Fig. 1a inset) with the engineering stress and strain measured continuously (see SM for details). The measurement protocol was calibrated using a material with a known $E$ value in this range relevant to MHPs; see SM and Fig. S1. Figures 1a and 1b present the engineering stress-strain curves from <100> $MAPbBr_3$ and $MAPbI_3$ bulk single-crystals, respectively. (The test ended because the crystals broke, with no evidence of yielding). From the linear fits to these curves the average $E_{<100>}$ ($= \sigma/\varepsilon$) for $MAPbBr_3$ and $MAPbI_3$ are estimated to be 13.1 ± 1.3 GPa and 10.6 ± 1.0 GPa, respectively,

indicating that these materials are quite compliant. (By comparison, average $E$ of Si and CdTe is ~160 GPa [23] and ~50 GPa, [24] respectively.) The trend in $E$, $MAPbBr_3$ > $MAPbI_3$, is consistent with what has been measured using indirect methods, and it is attributed to the same trend in bond strength: Pb-Br > Pb-I.[25] However, this measured $MAPbBr_3$ $E_{<100>}$ is overall much lower than that measured using indirect methods, whereas that for $MAPbI_3$ is similar to the one measured using nanoindentation by Sun, *et al*.[26] Since a calibrated direct method is used here to measure the $E_{<100>}$, we recommend that these values be used in the future as the best estimates. This direct $E$ measurement method could be extended to other orientations and other MHPs if high-quality cm-scale bulk single-crystal specimens can be synthesized and fabricated.

**Table 1**. Summary of experimentally measured $E$ of $MAPbBr_3$ and $MAPbI_3$ single-crystals.

| MHP | $E$ (GPa) | Method | Remarks | Ref. |
|---|---|---|---|---|
| $MAPbBr_3$ | 17.7 ± 0.6 | Nanoindentation | (100); CSM | [26] |
| | 19.6 ± 0.3 | Nanoindentation | (100); CSM | [27] |
| | 21.4 ± 4.0 | Nanoindentation | (100); dwell time 30 s | [28] |
| | 28.3(4) | Ultrasonic | <100>; from $C_{11}$ and $C_{12}$ | [29] |
| | 30.2 | Brillouin Scattering | <100>; from $C_{11}$ and $C_{12}$ | [30] |
| | 21.6 | Neutron Scattering | <100>; from $C_{11}$ and $C_{12}$ | [31] |
| | 28.2 | Brillouin Scattering | <100>; from $C_{11}$ and $C_{12}$ | [31] |
| | 26.3 | Photoacoustic | <100>; from $C_{11}$ and $C_{12}$ | [32] |
| | 13.1 ± 1.3 | Uniaxial Compression | <100>; direct measurement | This work |
| $MAPbI_3$ | 10.4 ± 0.8 | Nanoindentation | (100); CSM | [26] |
| | 14.3 ± 1.7 | Nanoindentation | (100); CSM | [27] |
| | 10.8 ± 2.7 | Nanoindentation | (100); dwell time 30 s | [28] |
| | 20.0 ± 1.5 | Nanoindentation | (100) | [33] |
| | 17.8 | Nanoindentation | (100); dwell time 0.5 s | [11] |
| | 12.7 | Nanoindentation | (100); dwell time 20 s | [11] |
| | 23.92 ± 3.63 | Nanoindentation | (100); dwell time 30 s | [34] |
| | 14.1 | Neutron Scattering | <100>; from $C_{11}$ and $C_{12}$ | [31] |
| | 10.6 ± 1.0 | Uniaxial Compression | <100>; direct measurement | This work |

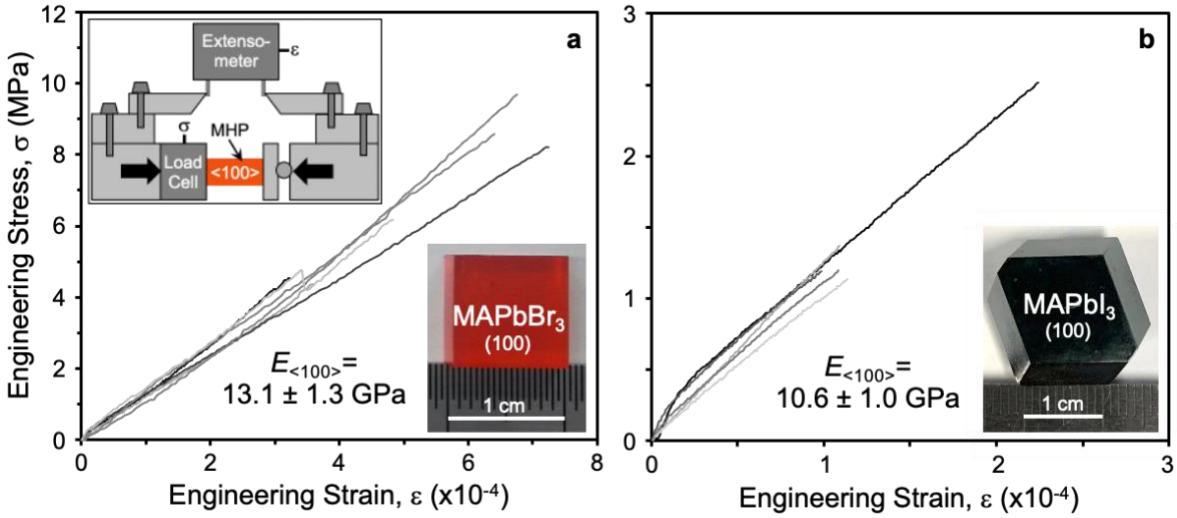


**Figure 1.** Engineering σ-ε responses from uniaxial compression of single-crystals (<100> direction): (a) $MAPbBr_3$ and (b) $MAPbI_3$. $E_{<100>}$ values estimated by linear-fitting; average and standard deviation of six measurements. Insets: schematic illustration of the mechanical testing apparatus (a), and photographs of cm-sized bulk single-crystal of $MAPbBr_3$ (a) and $MAPbI_3$ (b).

*Plasticity.* Plastic deformation of 'soft' semiconductors such as MHPs generates line (dislocations) and surface (stacking faults, twins) defects, which can adversely affect their optoelectronic properties.[15] Since the propensity for local plastic deformation in a material is quantified by its hardness ($H$), it is critically important to measure it accurately. To that end, systematic Vickers micro-indentation experiments were performed on (100) surfaces of the $MAPbBr_3$ and $MAPbI_3$ single-crystals to measure the $H$ values; see SM for the experimental details. Figures 2a and 2b present $H_{(100)}$ for $MAPbBr_3$ and $MAPbI_3$, respectively, which are independent of the applied indentation load ($P_M$) in the range studied. The following relation was used to calculate the $H$, which uses the projected area of the indentation impression:[35]

$$H = \frac{P_M}{2a^2}, \qquad (1)$$

where $2a$ is the length of the square impression diagonal. The average $H_{(100)}$ of $MAPbBr_3$ and $MAPbI_3$ is 0.54 ± 0.02 GPa and 0.76 ± 0.05 GPa, respectively, indicating that these materials are quite soft. (By comparison, average $H$ of Si and CdTe is ~14 GPa [36] and ~0.4 GPa,[37]

respectively.) The $MAPbBr_3$ < $MAPbI_3$ trend is consistent with what has been reported in the literature for $H_{(100)}$ using the nanoindentation method (Table 2): 0.30-0.36 GPa for $MAPbBr_3$ and 0.42-1.05 GPa for $MAPbI_3$. Vickers indentation is generally more reliable for bulk materials as it samples larger depth/area, and minimizes any undesirable surface and/or indentation-size effects common among nanoindentation methods. Also, both $MAPbBr_3$ and $MAPbI_3$ are known to be viscoplastic materials as they undergo significant nanoindentation creep at room temperature.[28] As such, the measured nanoindentation $H$ depends on the dwell time ($t_D$) at $P_M$.[11, 26, 28] If the Continuous Stiffness Measurement (CSM) mode is used in the nanoindentation tests, $t_D$ may not be relevant, but a correction for the effective nanoindentation load is needed for accurate $H$ measurement.[38] Figure 2c shows a decreasing trend in Vickers $H_{(100)}$ of $MAPbBr_3$ with $t_D$, whereas this trend in $MAPbI_3$ is not readily apparent. Therefore, shortest dwell time ($t_D$ ~0.5 s) after the full load is applied results in the best estimate of average $H_{(100)}$ values, as reported in Fig. 2a. Consistent with what has been reported in the literature (Tables 1 and 2), $MAPbBr_3$ is found to be stiffer than $MAPbI_3$, but $MAPbI_3$ is harder than $MAPbBr_3$. In this context, Sun, *et al.*[26] have suggested that the higher hardness of $MAPbI_3$ may be due to its lower symmetry (tetragonal), compared to $MAPbBr_3$ (cubic) at room temperature, where, generally, dislocation slip is relatively more difficult.

**Table 2**. Summary of experimentally measured $H$ of $MAPbBr_3$ and $MAPbI_3$ bulk single-crystals on (100) surface.

| MHP | $H_{(100)}$ (GPa) | Method | Remarks | Ref. |
|---|---|---|---|---|
| $MAPbBr_3$ | 0.31 ± 0.02 | Nanoindentation | $t_D$ 30 s | [26] |
| | 0.36 ± 0.01 | Nanoindentation | - | [27] |
| | 0.36 ± 0.03 | Nanoindentation | $t_D$ 30 s | [28] |
| | 0.54 ± 0.02 | Vickers Micro-indentation | $P_M$ 3.924 N; $t_D$ ~0.5 s | This work |
| $MAPbI_3$ | 0.42 ± 0.04 | Nanoindentation | $t_D$ 30 s | [26] |
| | 0.55 ± 0.12 | Nanoindentation | $t_D$ 30 s | [28] |
| | 0.57 ± 0.11 | Nanoindentation | - | [27] |
| | 0.58 | Nanoindentation | $t_D$ 0.5 s | [11] |
| | 0.48 | Nanoindentation | $t_D$ 20 s | [11] |
| | 1.0 ± 0.1 | Nanoindentation | - | [33] |
| | 1.05 ± 0.18 | Nanoindentation | $t_D$ 30 s | [34] |
| | 0.76 ± 0.05 | Vickers Micro-indentation | $P_M$ 3.924 N; $t_D$ ~0.5 s | This work |

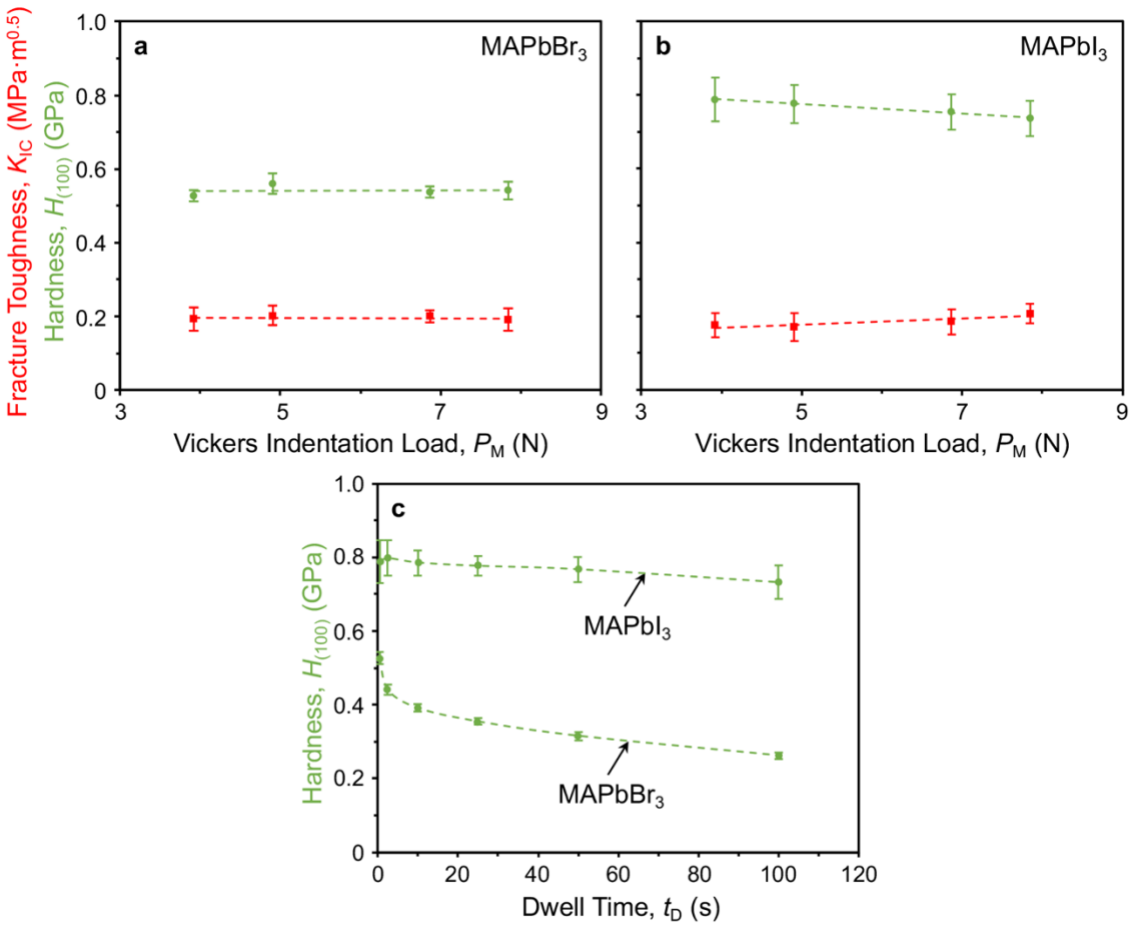


**Figure 2.** Micro-indentation (Vickers) $H_{(100)}$ and $K_{IC}$ as a function of $P_M$ of single-crystals ((100) surface): (a) $MAPbBr_3$ and (b) $MAPbI_3$. (c) $H_{(100)}$ of $MAPbBr_3$ and $MAPbI_3$ as a function of $t_D$. Average and standard deviation of 6-10 measurements; dashed lines are linear fits (a, b) or guide to the eye (c).

*Fracture.* The brittleness of MHPs is a major issue with regards to the mechanical reliability of PSCs. Cracking in MHP thin films not only blocks photocarriers and compromises the mechanical integrity of the device, but it also allows easy ingression of environmental species that contribute to the rapid degradation of the device. In this context, accurate measurement of the fracture toughness ($K_{IC}$), which quantifies the brittleness of the MHPs, is critically important for analyzing the mechanical reliability of PSCs. Here, Vickers micro-indentation can also be used to estimate the $K_{IC}$ of brittle solids.[35] The average indentation $K_{IC}$ of $MAPbBr_3$ and $MAPbI_3$ is estimated at $0.20 \pm 0.03$ MPa·m$^{0.5}$ and $0.18 \pm 0.03$ MPa·m$^{0.5}$, respectively, which is independent of $P_M$ (Fig. 2a). While anisotropy in the cracks emanating from the indentation were observed, these values

are for fracture along planes close to {110}. The above measured *E/H* ratios are used to calculate the $K_{IC}$ using the following:[35]

$$K_{\mathrm{IC}} = 0.016\left(\frac{E}{H}\right)^{0.5} Pc^{-1.5}, \qquad (2)$$

where 2*c* is the tip-to-tip length of the indentation-crack surface traces. While $K_{IC}$ of $MAPbBr_3$ has not been reported in the literature, the reported indentation $K_{IC}$ of $MAPbI_3$ bulk single-crystals are in the range 0.145-0.22 MPa·m$^{0.5}$.[11, 39] Considering that incorrect *E*/*H* ratios may have been used in the earlier calculations of $K_{IC}$, we recommend that the $K_{IC}$ values reported here be used in the future as the best estimates. (By comparison, average $K_{IC}$ of Si and CdTe is ~1 MPa·m$^{0.5}$ [40] and ~0.20 MPa·m$^{0.5}$,[41] respectively.) Clearly these MHPs are very brittle, as evinced by the facile edge-chipping of the single-crystals when handling them in the laboratory, where the critical chipping load scales with $K_{IC}$.[42] The toughness can also be expressed in terms of energy (plane stress), $G_C=K_{IC}^2/E$, which for $MAPbBr_3$ and $MAPbI_3$ is identical: ~3 J·m$^{-2}$ (cohesion). Since the fracture of these highly brittle materials, which lack any intrinsic or extrinsic toughening mechanisms as defined by Ritchie,[43] is entirely governed by surface energies, it appears that the specific surface energies ($\gamma_S=G_C/2$) of both $MAPbBr_3$ and $MAPbI_3$ are about the same: ~1.5 J·m$^{-2}$. (Note that, although these MHPs show extensive plasticity under the intense pressure of the indenter in a hardness test (low *H*), it has little relevance to the mode I fracture toughness, as is the case in highly brittle materials.[44])

<u>*Creep.*</u> As mentioned earlier, room-temperature nanoindentation creep (viscoplasticity) in $MAPbBr_3$ and $MAPbI_3$ single-crystals has been observed previously.[28] This has implications for time-dependent damage-accumulation and permanent shape-change of MHPs within PSCs, which is relevant to mechanical reliability of PSCs. Creep deformation also has implications on the *E* and *H* measurements using the popular nanoindentation method. Thus, systematic nanoindentation creep experiments were performed on (100) surfaces of $MAPbBr_3$ and $MAPbI_3$ bulk single-crystals using a nanoindenter unit that is not equipped with a CSM module. Figures 3a and 3b plot representative nanoindentation load (*P*)-displacement (*h*) loading-unloading curves for $MAPbBr_3$ and $MAPbI_3$, respectively, for peak-load ($P_M$ = 12 mN) and $t_D$ in the range 0.5-100 s (same loading and unloading rates of 2.4 mN·s$^{-1}$), confirming the creep effect. Only in the case of $MAPbBr_3$ and the shortest dwell time ($t_D$ = 0.5 s) the 'bowing' effect is observed in the unloading part of the *P*-*h* curve. Thus, those data cannot be used to extract *E* using the Oliver-Pharr model, which relies

on the proper fitting of the unloading part (elastic recovery) of the *P-h* curve.[45] The remainder of the unloading *P-h* data in Figs. 3a and 3b were used to extract *E* values, and are plotted in Fig. 3e, where the horizontal dashed lines represent the directly measured $E_{<100>}$ values from Figs. 1a and 1b. It is clear that the shortest dwell times result in more reliable *E* measurements using nanoindentation when the CSM module is not available. This may not be relevant when the CSM mode is used, where the *E* values are extracted from the material's response during loading with a superimposed small oscillatory load.[46]

The displacement (*h*) data in Figs. 3a and 3b are replotted as a function of time (*t*) in Figs. 3c and 3d, respectively. A comparison of the creep data, between onset of dwell at peak load (vertical dashed line) to onset of unloading (arrows), shows that $MAPbBr_3$ creeps significantly more than $MAPbI_3$, consistent with what has been observed before.[28] To analyze this further, the *h*(*t*) data were used to extract 'equivalent' steady-state strain-rate ($\dot{\varepsilon}_i$) and applied stress ($p_M$) plots using a procedure described by Ginder, *et al*.,[47] and are shown in Fig. 4. Here, $\dot{\varepsilon}_i = 0.36\,\dot{h}/h$ and $p_M = 0.04P_M/h^2$. Although the $\dot{\varepsilon}_i$ range is relatively small (~1.5 decade), the extracted steady-state $\dot{\varepsilon}_i$-$p_M$ data can be fitted to the conventional creep relation at a constant temperature:[47]

$$\dot{\varepsilon}_i = Ap_M^n, \qquad (3)$$

where *A* is a constant, and *n* is the stress exponent, which is ~8 and ~10 for $MAPbBr_3$ and $MAPbI_3$, respectively. Reyes-Martinez, *et al*.[28] have extracted *n* values of 3.78 and 4.71 for $MAPbBr_3$ and $MAPbI_3$, respectively, from their nanoindentation creep data, but using a different method. Once again, Fig. 4 confirms that $MAPbI_3$ is more creep-resistant than $MAPbBr_3$, and yields better estimates of *n*. In general, such high *n* values imply that dislocation glide and climb (power law) creep mechanism is dominant in the material, where the 'glide' part is controlled by plasticity (*H*) and the 'climb' part is controlled by atomic/ionic diffusion.[48] Since room-temperature ion-migration in MHPs is facile,[49] it is reasonable to conclude that nanoindentation creep in $MAPbBr_3$ and $MAPbI_3$ occurs *via* dislocation glide and climb. However, room-temperature ion-migration in $MAPbI_3$ is more facile than $MAPbBr_3$, which has been used to explain the generally observed better environmental stability of the latter.[50] The fact that $MAPbI_3$ is more creep-resistant despite more facile diffusion suggests that its higher *H* (glide) plays a more dominant role compared with diffusion-assisted climb, under the combination of conditions in room-temperature nanoindentation creep: relatively high stress and low temperature. (By comparison, Si does not

exhibit nanoindentation creep at room temperature,[51] whereas CdTe shows modest nanoindentation creep.[52]) Further elucidation of creep deformation mechanisms in MHPs under different stress-temperature combinations await creep experiments performed in uniaxial compression of bulk MHPs.

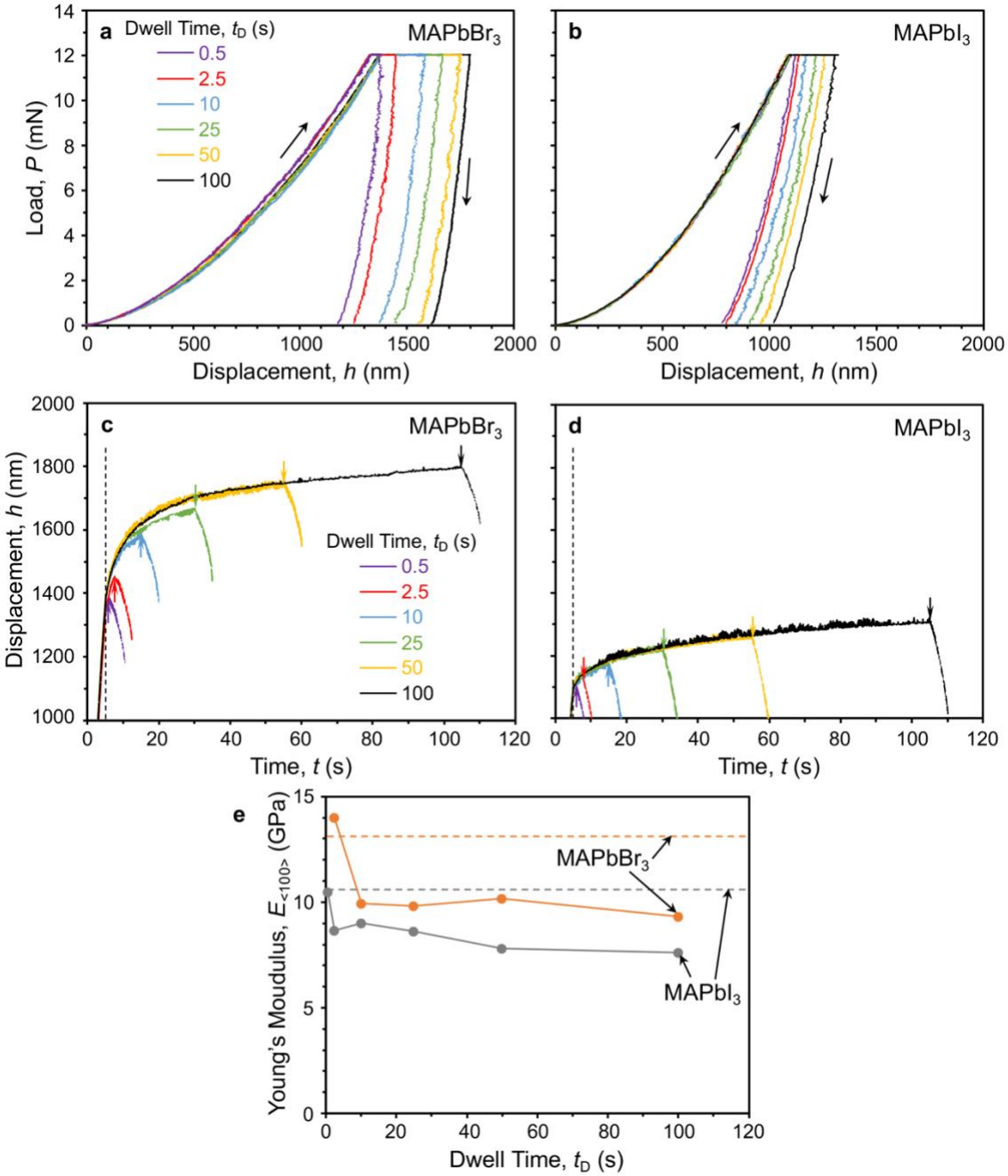


**Figure 3.** Nanoindentation (Berkovich) loading-unloading (indicated by arrows) *P-h* responses of single-crystals ((100) surface) as a function of $t_D$: (a) $MAPbBr_3$ and (b) $MAPbI_3$. Corresponding *h-t* responses as

a function of $t_D$: (c) $MAPbBr_3$ and (d) $MAPbI_3$. Vertical dashed lines and arrows mark dwell-onset and unloading-onset, respectively. (e) $E_{<100>}$ of $MAPbBr_3$ and $MAPbI_3$ extracted from the unloading part of the *P-h* curves in (a) and (b) as a function of $t_D$. Solid lines connect the data points; horizontal dashed lines are corresponding directly measured $E_{<100>}$ of $MAPbBr_3$ and $MAPbI_3$ in Figs. 1a and 1b, respectively.

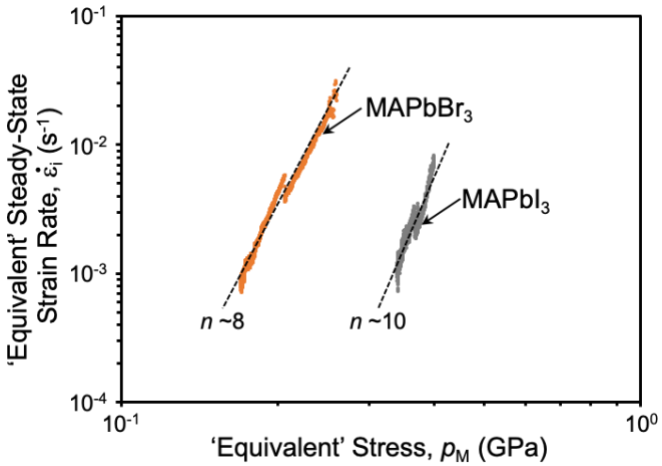


**Figure 4.** The 'equivalent' steady-state $\dot{\varepsilon}_i$-$p_M$ response extracted from the nanoindentation creep data for $MAPbBr_3$ and $MAPbI_3$ in Figs. 3c and 3d, respectively. The *n* values are estimated from linear fits to the data (dashed lines).

In summary, accurate measurements of relevant mechanical properties of MHPs are critically important for analyzing mechanical reliability of PSCs in the future. To that end, elasticity, plasticity, fracture, and creep behaviors in $MAPbBr_3$ and $MAPbI_3$ bulk single-crystals are systematically studied. We have directly measured the Young's modulus $E_{<100>}$ of $MAPbBr_3$ and $MAPbI_3$ using bulk uniaxial compression, which is 13.1 ± 1.3 and 10.6 ± 1.0 GPa, respectively. The Vickers microhardness $H_{(100)}$ of $MAPbBr_3$ and $MAPbI_3$ is 0.54 ± 0.02 GPa and 0.76 ± 0.05 GPa, respectively. The Vickers micro-indentation fracture toughness $K_{IC}$ of $MAPbBr_3$ and $MAPbI_3$ is estimated at 0.20 ± 0.03 $MPa{\cdot}m^{0.5}$ and 0.18 ± 0.03 $MPa{\cdot}m^{0.5}$, respectively. The stress-exponent, *n*, extracted from nanoindentation creep data is ~8 and ~10 for $MAPbBr_3$ and $MAPbI_3$, respectively. All these properties are best estimates and are recommended for use in future mechanical reliability analyses of MHPs and PSCs.

**Acknowledgements**

The funding from the work at Brown University by the National Science Foundation (grant no. DMR-2102210), Office of Naval Research (grant no. N00014-20-1-2574), and the Department of Energy Basic Energy Sciences (grant No. DE-SC0018113) is gratefully acknowledged. The work at Shaanxi Normal University was supported by the National Natural Science Foundation of China (62104137, 62174103), the China National Postdoctoral Program for Innovative Talents (BX2021173), the National Key Research and Development Program of China (2017YFA0204800), the DNL Cooperation Fund CAS (DNL180311), the 111 Project (B21005), and the Changjiang Scholar and Innovative Research Team (IRT_14R33).

**References**

[1] A.K. Jena, A. Kulkarni, T. Miyasaka, Halide perovskite photovoltaics: background, status, and future prospects, Chem. Rev. 119 (2019) 3026-3103.

[2] T. Miyasaka, Perovskite Photovoltaics and Optoelectronics: From Fundamentals to Advanced Applications, Wiley-VCH, Weinheim, Germany, 2021.

[3] A.W.Y. Ho-Baillie, J.H. Zheng, M.A. Mahmud, F.J. Ma, D.R. McKenzie, M.A. Green, Recent progress and future prospects of perovskite tandem solar cells, Appl. Phys. Rev. 8 (2021) 041307.

[4] F. Fu, J. Li, T.C.J. Yang, L.H. Liang, A. Faes, Q. Jeangros, C. Ballif, Y. Hou, Monolithic perovskite-silicon tandem solar cells: from the lab to fab?, Adv. Mater. 34 (2022) 2106540.

[5] J. Yan, T.J. Savenije, L. Mazzarella, O. Isabella, Progress and challenges on scaling up of perovskite solar cell technology, Sustain. Ener. Fuels. 6 (2022) 243-266.

[6] C.C. Boyd, R. Cheacharoen, T. Leijtens, M.D. McGehee, Understanding degradation mechanisms and improving stability of perovskite photovoltaics, Chem. Rev. 119 (2019) 3418-3451.

[7] S.P. Dunfield, L. Bliss, F. Zhang, J.M. Luther, K. Zhu, M.F.A.M. van Hest, M.O. Reese, J.J. Berry, From defects to degradation: a mechanistic understanding of degradation in perovskite solar cell devices and modules, Adv. Ener. Mater. 10 (2020) 1904054.

[8] W. Xiang, S.Z. Liu, W. Tress, A review on the stability of inorganic metal halide perovskites: challenges and opportunities for stable solar cells, Ener. Environ. Sci. 14 (2021) 2090-2113.

[9] N. Rolston, B.L. Watson, C.D. Bailie, M.D. McGehee, J.P. Bastos, R. Gehlhaar, J.-E. Kim, D. Vak, A.T. Mallajosyula, G. Gupta, A.D. Mohite, R.H. Dauskardt, Mechanical integrity of solution-processed perovskite solar cells, Extreme Mech. Lett. 9 (2016) 353-358.

[10] J.-H. Kim, I. Lee, T.-S. Kim, N. Rolston, B.L. Watson, R.H. Dauskardt, Understanding mechanical behavior and reliability of organic electronic materials, MRS Bull. 42 (2017) 115-123.

[11] C. Ramirez, S.K. Yadavalli, H.F. Garces, Y. Zhou, N.P. Padture, Thermo-mechanical behavior of organic-inorganic halide perovskites for solar cells, Scripta Mater. 150 (2018) 36-41.

[12] P. Holzhey, M. Saliba, A full overview of international standards assessing the long-term stability of perovslite solar cells, J. Mater. Chem. A 6 (2018) 21794-21808.

[13] L.-J. Li, S.-J. Sun, Y. Qin, K. Li, W. Li, Mechanical properties of hybrid organic-inorganic perovskites, Coord. Chem. Rev. 391 (2019) 15-29.

[14] D. Liu, D. Luo, A.N. Iqbal, K.W.P. Orr, T.A.S. Doherty, Z.-H. Lu, S.D. Stranks, W. Zhang, Strain analysis and engineering in halide perovskite photovoltaics, Nat. Mater. 20 (2021) 1337-1346.

[15] Q. Tu, D. Kim, M. Shyikh, M.G. Kanatzidis, Mechanics-coupled stability of metal-halide perovskites, Matter 4 (2021) 2765-2809.

[16] S.K. Yadavalli, Z. Dai, H. Zhou, Y. Zhou, N.P. Padture, Facile crack-healing in organic-inorganic halide perovskite thin films, Acta Mater. 187 (2020) 112-121.

[17] N. Rolston, K.A. Bush, A.D. Printz, A. Gold-Parker, Y. Ding, M.F. Toney, M.D. McGehee, R.H. Dauskardt, Engineering stress in perovskite solar cells to improve stability, Adv. Ener. Mater. 8 (2018) 1802139.

[18] M. Dailey, Y. Li, A.D. Printz, Residual film stresses in perovskite solar cells: origins, effects, and mitigation strategies, ACS Omega 6 (2021) 30214-30223.

[19] J. Feng, Mechanical properties of hybrid organnic-inorganic $CH_3NH_3BX_3$ (B = Sn, Pb; X = Br, I) perovskite solar cell absorbers, APL Mater. 2 (2014) 081801.

[20] M. Faghihnasiri, M. Izadifard, M.E. Ghazi, DFT study of mechanical properties and stability of cubic methylammonium lead halide perovskites ($CH_3NH_3PbX_3$, X = I, Br, Cl), J. Phys. Chem. C 121 (2017) 27059-27070.

[21] C. Ge, M. Hu, P. Wu, Q. Tan, Z. Chen, Y. Wang, J. Shi, J. Feng, J. Ultralow thermal conductivity and ultrahigh thermal expansion of single-crystal organic-inorganic hybrid perovskite $CH_3NH_3PbX_3$ (X = Cl, Br, I), Phys. Chem. C 122 (2018) 15973-15978.

[22] Y. Liu, Y. Zhang, X. Zhu, Z. Yang, W. Ke, J. Feng, X. Ren, K. Zhao, M. Liu, M.G. Kanatzidis, S. Liu, Inch-sized high-quality perovskite single crystals by suppressing phase segregation for light-powered integrated circuits, Sci. Adv. 7 (2021) eabc8844.

[23] M.A. Hopcroft, W.D. Nix, T.W. Kenny, What is the Young's modulus of silicon?, J. MEMS 19 (2010) 229-238.

[24] E. Deligoz, K. Colakoglu, Y. Ciftci, Elastic, electronic, and lattice dynamical properties of CdS, CdSe, and CdTe, Phys. B 373 (2006) 14-130.

[25] S. Sun, F.H. Isikgor, Z. Deng, F. Wei, G. Kieslich, P.D. Bristowe, J. Ouyang, A.K. Cheetham, Factors influencing the mechanical properties of formamidinium lead halides and related hybrid perovskites, ChemSusChem 10 (2017) 3740-3745.

[26] S. Sun, Y. Fang, G. Kieslich, T.J. White, A.K. Cheetham, Mechanical properties of organic-inorganic halide perovskites, $CH_3NH_3PbX_3$ (X = I, Br and Cl), by nanoindentation, J. Mater. Chem. A 3 (2015) 18450-18455.

[27] Y. Rakita, S.R. Cohen, N.K. Kedem, G. Hodes, D. Cahen, Mechanical properties of $APbX_3$ (A = Cs or $CH_3NH_3$; X = I or Br) perovskite single crystals, MRS Commun. 5 (2015) 623-629.

[28] M.A. Reyes-Martinez, A.L. Abdelhady, M.I. Saidaminov, D.Y. Chung, O.K. Bakr, M.G. Kanatzidis, W.O. Soboyejo, Y.-L. Loo, Time-dependent mechanical response of $APbX_3$ (A = Cs, $CH_3NH_3$; X = I, Br) single crystals, Adv. Mater. 29 (2017) 1606556.

[29] A.M. Lomonosov, X. Yan, C. Sheng, V.E. Gusev, Exceptional elastic anisotropy of hybrid organic–inorganic perovskite $CH_3NH_3PbBr_3$ measured by laser ultrasonic technique, Phys. Stat. Solidi Rap. Res. Lett. 10 (2016) 606-612.

[30] A. Letoublon, S. Paofai, B. Ruffle, P. Bourges, B. Hehlen, T. Michel, C. Ecolivet, O. Durand, S. Cordiier, C. Katan, J. Even, Elastic constants, optical phonons, and molecular relaxations in the high temperature plastic phase of the $CH_3NH_3PbBr_3$ hybrid perovskite, J. Phys. Chem. Lett. 7 (2016) 3776-3784.

[31] A.C. Ferreira, A. L´etoublon, S. Paofai, S. Raymond, C. Ecolivet, B. Ruffle', S. Cordier, C. Katan, M.I. Saidaminov, A.A. Zhumekenov, O.M. Bakr, J. Even, P. Bourges, Elastic softness of hybrid lead halide perovskites, Phys. Rev. Lett. 121 (2018) 085502.

[32] T. Zhang, X.-Y. Liu, C. Tao, X. Xu, X.-J. Liu, Noncontact evaluation of full elastic constants of perovskite $MAPbBr_3$ *via* photoacoustic eigenspectrum analysis in one test, Sci. Rep. 10 (2020) 9994.

[33] M. Spina, A. Karimi, W. Andreoni, C.A. Pignedoli, B. Nafradi, L. Forro, E. Horvath, Mechanical signatures of degradation of the photovoltaic perovskite $CH_3NH_3PbI_3$ upon water vapor exposure, Appl. Phys. Lett. 110 (2017) 121903.

[34] I. Spanopoulos, I. Hadar, W. Ke, Q. Tu, M. Chen, H. Tsai, Y. He, G. Shekhawat, V.P. Dravid, M.R. Wasielewski, A.D. Mohite, C.C. Stoumpos, M.G. Kanatzidis, Uniaxial expansion of the 2D Ruddlesden-Popper perovskite family for improved environmental stability, J. Am. Chem. Soc. 141 (2019) 5518-5534.

[35] B.R. Lawn, Fracture of Brittle Solids, Cambridge University Press, Cambridge, U.K., 1993.

[36] R. Berriche, Vickers hardness from plastic energy, Scripta Mater. 32 (1995) 617-620.

[37] I. Yonenaga, T. Suzuki, Indentation hardnesses of semiconductors and a scaling rule, Philos. Mag. Lett. 82 (2002) 535-542.

[38] P.S. Phani, W.C. Oliver, G.M. Pharr, On the effective load during nanoindentation creep testing with continuous stiffness measurement (CSM), J. Mater. Res. 36 (2021) 1740-1750.

[39] N. Rolston, A.D. Printz, J.M. Tracy, H.C. Weerasinghe, D. Vak, L.J. Haur, A. Priyadarshi, N. Mathews, D.J. Slotcavage, M.D. McGehee, R.E. Kalan, K. Zielinski, R.L. Grimm, H. Tsai, W. Nie, A.D. Mohite, S. Gholipour, M. Saliba, M. Grätzel, R.H. Dauskardt, Effect of cation composition on the mechanical stability of perovskite solar cells, Adv. Ener. Mater. 8 (2018) 1702116.

[40] M. Sebastiani, K.E. Johanns, E.G. Herbert, G.M. Pharr, Measurement of fracture toughness by nanoindentation methods: Recent advances and future challenges, Curr. Op. Sol. Stat. Mater. Sci. 19 (2015) 324-333.

[41] B. Wermke, M. Petzold, Experimental determination of the fracture toughness of CdTe, Cryst. Res. Technol. 25 (1990) K121-K124.

[42] B.R. Lawn, Chipping: a pervasive presence in nature, science and technology, J. Mater. Sci. 56 (2021) 8396-8405.

[43] R.O. Ritchie, Toughening materials: enhancing resistance to fracture, Philos. Trans. Roy. Soc. A 379 (2021) 20200437.

[44] W.C. Oliver, G.M. Pharr, An improved technique for determining hardness and elastic modulus using load and displacement sensing indentation experiments, J. Mater. Res. 7 (1992) 1564-1583.

[45] P.S. Phani, W.C. Oliver, G.M. Pharr, Measurement of hardness and elastic modulus by load and depth sensing indentation: improvements to the technique based on continuous stiffness measurement, J. Mater. Res. 36 (2021) 2137-2153.

[46] R.S. Ginder, W.D. Nix, G.M. Pharr, A simple model for indentation creep, J. Mech. Phys. Sol. 112 (2018) 552-562.

[47] J. Poirier, Creep of Crystals, Cambridge University Press, Cambridge, UK, 1985.

[48] X. Yan, W. Fan, F. Cheng, H. Sun, C. Xu, L. Wang, Z. Kang, Y. Zhang, Ion migration in hybrid perovskites: classification, identification, and manipulation, Nano Today 44 (2022) 101503.

[49] L. McGovern, M.H. Futscher, L.A. Muscarella, B. Ehler, Understanding the stability of $MAPbBr_3$ versus $MAPbI_3$: suppression of methylammonium migration and reduction of halide migration, J. Phys. Chem. Lett. 11 (2020) 7127-7132.

[50] S.E. Grillo, M. Ducarroir, M. Nadal, E. Tournie, J.-P. Faurie, Nanoindentation of Si, GaP, GaAs and ZnSe single crystals, J. Phys. D: Appl. Phys. 36 (2003) L5-L9.

[51] M. Pang, D.F. Bahr, K.G. Lynn, Effects of Zn addition and thermal annealing on yield phenomena of CdTe and $Cd0_{.96}Zn_{0.04}Te$ single crystals by nanoindentation, Appl. Phys. Lett. 82 (2003) 1200-1202.